Journal of the Society for Information Display

WILEY

SPECIAL SECTION PAPER OPEN ACCESS

Study of Far-Field Electroluminescence Emission to Enhance Micro-LED Performance

Fabian Rol | Stéphane Altazin | Nicolas Michit | Bastien Miralles | Clément Ballot | Bernard Aventurier | Paolo De Martino | Patrick Le Maitre | Julia Simon

Univ. Grenoble Alpes, CEA LETI, Minatec, Grenoble, France

Correspondence: Fabian Rol (fabian.rol@cea.fr)

Received: 28 March 2025 | **Revised:** 18 June 2025 | **Accepted:** 25 August 2025

Funding: This work was supported by the French Public Authorities.

Keywords: AR/VR | far field | GaN | micro-display | micro-LED | optical cavity | optical communication

ABSTRACT

This study investigates the angular dependence of far-field electroluminescence (EL) emission in InGaN/GaN LEDs and micro-LEDs to enhance their performance for micro-display and visible optical communication applications. We developed a measurement setup to analyze far-field EL emission across various wavelengths and compared the results with 1D optical simulations. This approach allowed us to observe the well-known dependence of emission directivity and light extraction efficiency (LEE) on the structural parameters of flip-chip LEDs, particularly the thicknesses of p-GaN and n-GaN layers, and to quantify the impact of total thickness variation resulting from wafer thinning processes. Using larger LEDs, the test vehicle offers a valuable tool for designing micro-LEDs with the desired directivity and for process monitoring. We also observed that the angular dependence of far-field emission varies with the applied bias and demonstrated how this could affect wafer-level micro-LED characterizations. Finally, we showed that the far-field EL emission of micro-LEDs progressively deviates from the description by a 1D optical cavity alone, suggesting an increasing influence of the limited size and necessitating 3D-FDTD simulations to accurately model both vertical cavity and sidewall effects. However, for sizes down to 5 μm, the directivity predicted by a 1D model seems roughly preserved.

1 | Introduction

The advanced developmental stage of InGaN/GaN LEDs characterized by their high efficiency, brightness, and robustness, resulting from their extensive development in the field of lighting, highlights their potential for micro-display applications, particularly for augmented reality and virtual reality (AR/VR). The need for a magnifying optical system to make the micro-LED-based pixels visible to the eye makes it desirable for them to have directional emission, as the system will likely be constrained by a limited numerical aperture. In addition, new applications of InGaN/GaN micro-LEDs are emerging [1]. In the field of visible optical communication, it would require the coupling of micro-LED emission in a waveguide of limited numerical aperture [2–5]. In this context, it seems important to understand and control the angular dependence of the far-field electroluminescence (EL) emission of micro-LEDs [6].

This paper presents experimental and simulated results of the emission diagram of macro-LEDs and micro-LEDs and the influence of various parameters on their emission directivity including epi-structure design, integration process, injected current density, and dimensions. By accurately measuring far-field emission of large LEDs (considered infinite) across

Fabian Rol and Stéphane Altazin contributed equally to this work.

various wavelengths, we can reliably fit experimental data, which are useful for optimizing both the directivity and light extraction efficiency (LEE) of micro-LEDs. Indeed, to properly model the impact of the limited size of micro-LEDs on their directivity, or to control their emission properties by integrating micro- or nano-optics on top of the devices, it is necessary to maintain a test vehicle on the micro-LED wafer to monitor the impact of optical cavities. This approach should enable us to refine the design and enhance the overall performance of micro-LEDs tailored for specific applications.

2 | Micro-LED Far-Field Characterizations and Simulations

2.1 | Fabricated Micro-LEDs

CEA-LETI has worked extensively for several years in the development of micro-LED fabrication for micro-display application [7, 8] and more recently for data communication [2, 3]. This study of the angular dependence of the far-field EL emission of micro-LEDs was conducted on individual disk micro-LEDs ranging in size from 200 µm down to 1.25 µm (cf., Figure 1b). They were part of a large variety of devices including micro-LEDs of various shapes and sizes, micro-displays, and matrices of different forms. They were realized in a CMOS-compatible cleanroom and integration flow and made from commercial LED epistructures grown on 200 mm silicon wafers. The schematic of these micro-LEDs is presented in Figure 1a. Their fabrication begins with metal–metal wafer bonding onto a silicon (100) carrier wafer followed by substrate removal and thinning of the GaN buffer using reactive ion etching. The entire process is conducted in a 200 mm format. The carrier wafer is only used to realize test structures but could be replace by an ASIC for final applications. We benefit from the maturity and resolution of processes made in 200 mm, and, with this whole-wafer transfer approach, we are not limited by any alignment processes beyond those performed in lithography tools. The metallic layers used for bonding also serve as the electrical p-contact and backside mirror. The mesas, which define the micro-LED shapes, are created using chlorine-based dry etching. They are then passivated to reduce dangling bonds and ensure electrical insulation. The sidewalls are covered by aluminum to prevent lateral light emission, which would lead in a micro-display to the so-called cross talk. Finally, after a planarization process with SiO_2, the last steps involve creating the contacts, connections, and pads [3].

2.2 | Far-Field Emission Measurement

We use a modified epi-fluorescence microscope to map the Fourier plane [9] of a micro-LED EL emission. The setup allows us to electrically drive micro-LEDs with probes directly on the 200-mm wafer and perform accurate angle calibration. The advantage of imaging the Fourier plane over a goniometric approach is that it captures all emission directions simultaneously, significantly reducing integration time. This

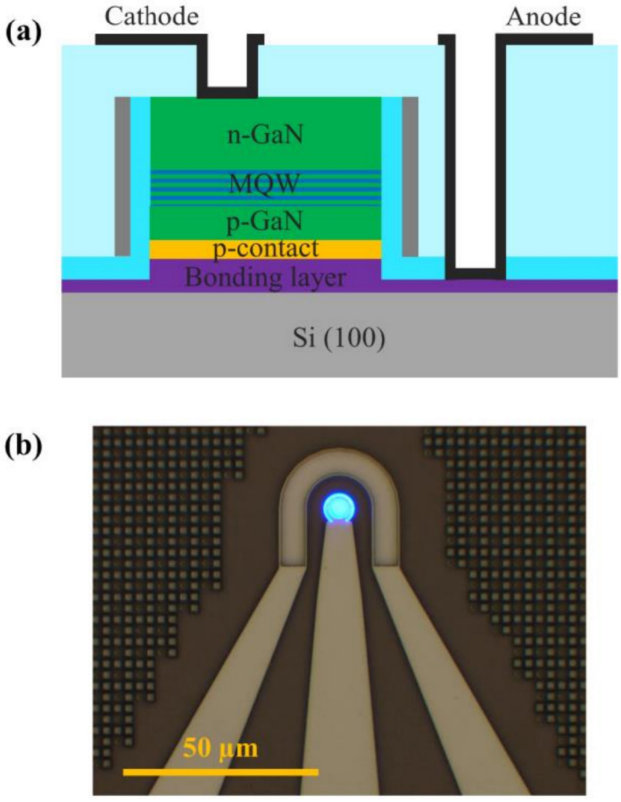

FIGURE 1 | (a) Cross-sectional schematic of micro-LEDs featuring a bottom reflective p-contact and a lateral mirror to prevent crosstalk. (b) Blue micro-LED with a diameter of 5 µm under EL emission.

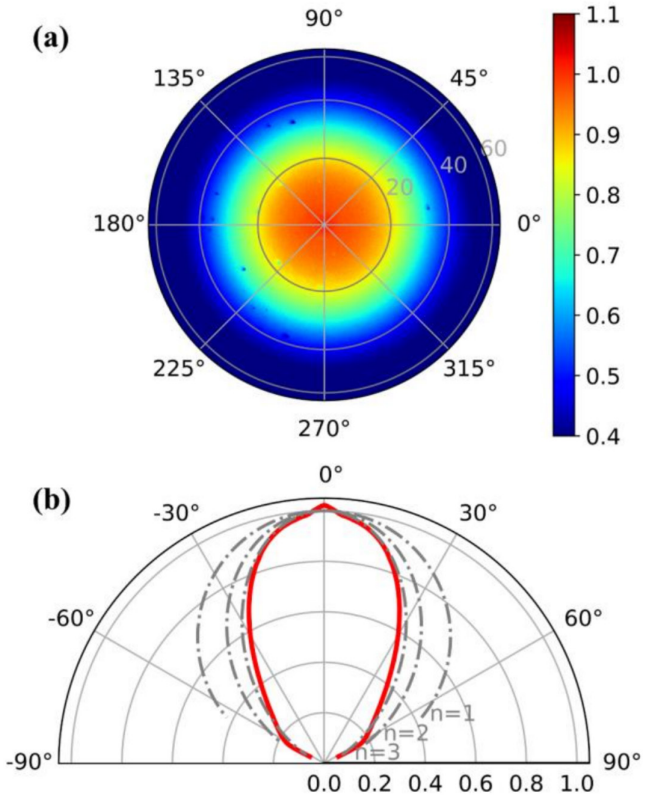

FIGURE 2 | Measurement and data processing to extract the angular dependence of far-field emission. (a) Fourier plane image of a 200-µm LED EL emission. (b) Circular averaging providing the emission diagram in red, compared to $cos\theta^n$ in gray with $n = 1, 2, 3$ ($n = 1$ corresponds to Lambertian emission).

is crucial for very small light emitters like micro-LEDs, which emit very low optical power due to their limited size. Figure 2a illustrates the LED EL intensity measured by the monochromatic CMOS detector while imaging the back focal plane of a 100× microscope objective (NA = 0.9). Each point on this map corresponds to a direction of emission, ranging from 0° at the center of the disk to a limit angle imposed by the numerical aperture of the objective, which is close to 64°. After angular calibration, this intensity mapping is circularly averaged to obtain the emission diagram shown in Figure 2b. The angular dependence of the far-field emission of this 200-μm LED is plotted in red, along with $\cos\theta^n$ in gray with $n = 1, 2, 3$ (where $n = 1$ corresponds to Lambertian emission). In this particular example, the emission is directional, which is desirable for several applications of micro-LEDs.

This setup also allows us to filter the EL emission using band-pass DBR filters with a full width at half maximum (FWHM) of 10 nm. In the following paragraphs, we will see that this wavelength decomposition makes the comparison between 1D simulations and experiments very accurate and can, for example, provide valuable information about the impact of optical cavities on emission directivity.

2.3 | Simulations

Due to the presence of a mirror on the p-GaN side of flip-chip micro-LEDs, as depicted in Figure 1a, 1D optical cavity effects can occur [10–12]. These effects depend on the position of the emitting dipoles within the structure and can significantly influence the angular dependence of the LED far-field EL emission. To reproduce these effects, simulations were performed using Setfos 5.2 software from Fluxim AG. This software is based on the dipole emission model within an infinite micro-cavity, as described in [13]. This semi-analytical description enables very fast simulation making fitting possible. For our LED model, to simplify the simulation and reduce the number of fitting parameters, we assumed that emission occurs only at a single depth in the LED stack. This assumption is based on the fact that in InGaN/GaN LEDs, the emission is generally considered to originate from the first quantum well (QW) on the p-GaN side [14]. Additionally, only horizontally aligned dipoles were considered in this simulation, as InGaN QW are expected to emit unpolarized light towards the c-axis but linearly polarized orthogonal to it [15, 16].

For the fitting procedure, we allowed both p-GaN and n-GaN thicknesses to be freely adjustable parameters, as described in Figure 3a. There are 25 nm of nid-GaN on both sides of the plane of dipoles, making the distance between the QW and the mirror equal to p-GaN + 25 nm, and the distance between the QW and the GaN/SiO2 interface equal to n-GaN + 25 nm.

Figure 3b clearly illustrates that the angular dependence of the normalized radiance varies significantly with the emission wavelength. This highlights the importance of being able to measure the wavelength dependence of the far-field emission. By decomposing the emission spectrally, we can achieve a highly sensitive fit between experimental data and the

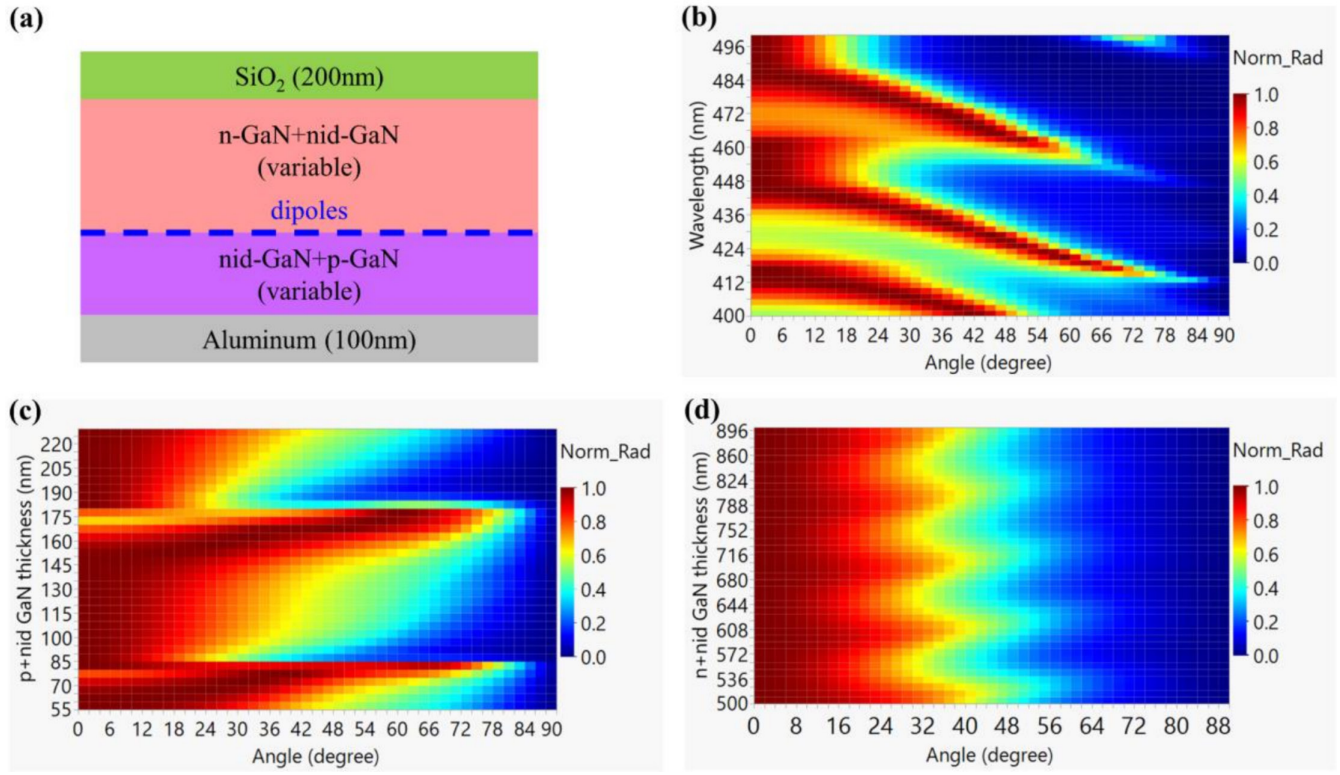

FIGURE 3 | (a) Simplified structure used for the 1D Setfos simulations. (b–d) Normalized radiance displayed in color plots as a function of the angle of far-field EL emission and (b) the emission wavelength, (c) the thickness of n-GaN + nid-GaN, and (d) the thickness of p-GaN + nid-GaN (nid-GaN = 25 nm). The normalization to the maximum is done per horizontal line to be comparable to the far-field measurements, similar to Figure 2b, which are also normalized to the maximum of intensity.

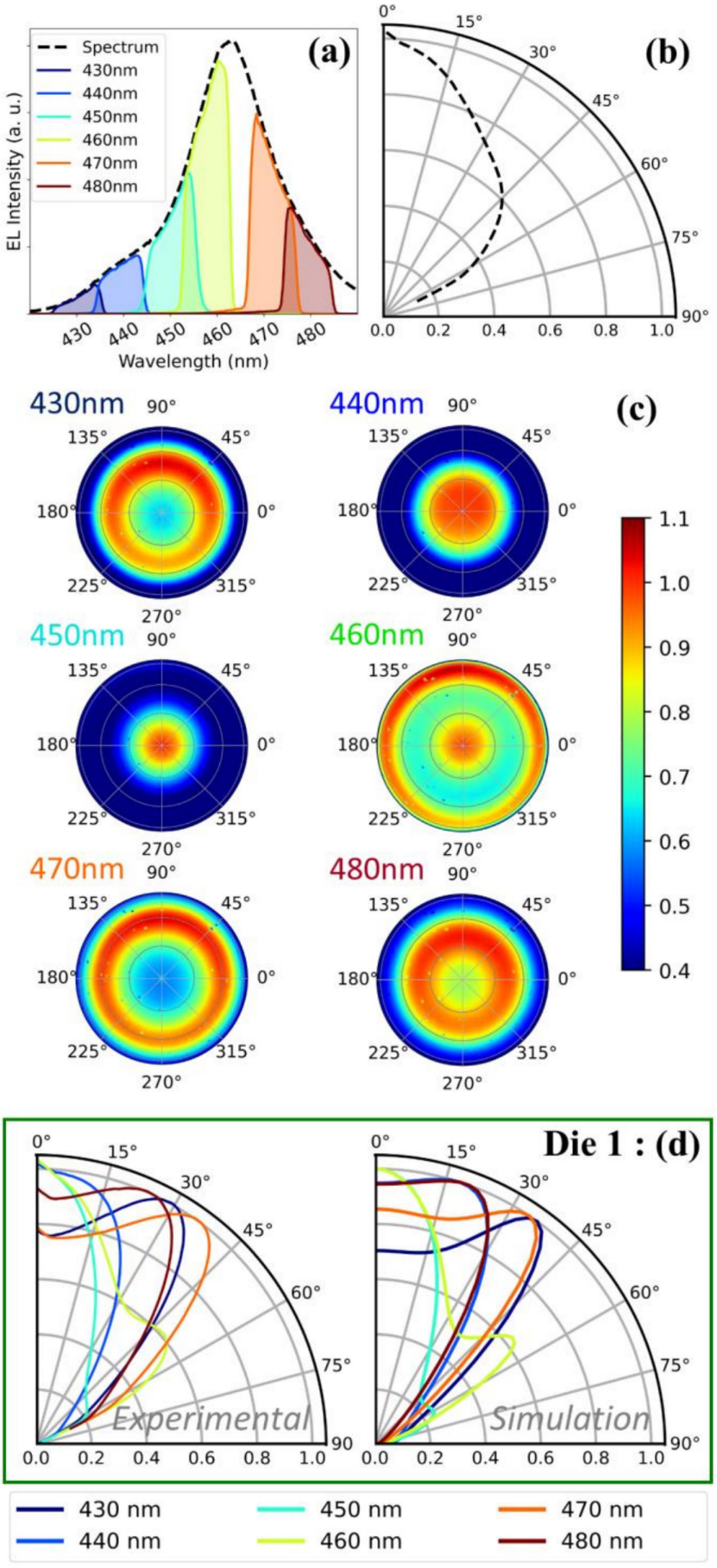

FIGURE 4 | Legend on next page.

FIGURE 4 | (a) EL spectrum of a 200-μm disk LEDs from Die 1, driven at approximatively 30A/cm^2 (black dotted line), and filtered emission between 430 and 480 nm (FWHM ~ 10 nm) (color lines). (b) Angular dependence of the far-field emission of the entire spectrum. (c) Emission diagrams plotted in the 2D space (θ, ϕ) for each wavelength slice. (d) Circularly averaged emission diagrams at the various wavelengths. The experimental data on the left are well described by the Setfos simulation on the right with the following thicknesses: p-GaN + nid-GaN = 202 nm, n-GaN + nid-GaN = 634 nm.

model described in Figure 3a, enabling precise adjustments of n-GaN and p-GaN thicknesses and validation of the 1D model. This kind of approach was previously used in the OLED community to analyze the recombination zone inside the emissive layer; see, for example, [17]. Figure 3c and Figure 3d precisely describe the variation in the angular dependence of the normalized radiance with the thickness of p-GaN + nid-GaN and n-GaN + nid-GaN, respectively. The simulations clearly show that the p-GaN thickness has a stronger impact on the directivity of emission than the n-GaN thickness. However, as we will see later, it is important to remember that for practical applications, in addition to directivity, we must also consider the absolute LEE.

2.4 | Emission Wavelength Dependence of Far-Field Emission

Figure 4 presents an example of experimental measurements that illustrate the impact of the emission wavelength on the angular dependence of the EL far-field emission of a macro-LED when optical cavity effects occur. Figure 4b corresponds to the emission diagram of the entire spectrum (plotted as a black dotted line in Figure 4a). Figure 4c represents the far-field emission diagrams plotted in the 2D space (θ, ϕ) for each wavelength slice presented in Figure 4a. Finally, Figure 4d represents the circularly averaged emission diagrams from Figure 4c and the comparison to the best-fitted simulation. The strong variations observed in the experimental data for the different wavelengths are rather well fitted by the model. In these simulations, an automatic fit is performed on a single wavelength, but the results presented consider the shape of the filtered spectra to better reflect reality. To achieve a better match between experiment and simulation, we may need a less simplified model, a more precise determination of the refractive indices of the different layers, and a more complex distribution of the emitting dipoles at various depths within the active region to account for possible injection through the V-pits.

3 | Characterization of Far-Field Emission in the Context of Micro-LED Development

This section explores how characterizing the angular dependence of far-field emission can help in studying and designing micro-LEDs. We begin the study with 200-μm LEDs, which can be considered "infinite" compared to micro-LEDs. In this context, cavity effects are well described by 1D Setfos simulations. Leveraging wavelength decomposition for accurate fitting, we investigate the impact of n-GaN and p-GaN thicknesses on the angular distribution of far-field emission. We emphasize that this experimental method provides a valuable tool for obtaining insights about emission directivity and LEE. It allows us to adjust the model parameters and ideally maximize LEE within the numerical aperture required by the application. Our characterization also reveals that the angular dependence of the far-field emission varies with current density, impacting the current dependence of the external quantum efficiency (EQE) during on-wafer characterization with limited numerical aperture collection. Finally, we apply these techniques to assess the impact of micro-LED size on the emission diagram.

3.1 | n-GaN and p-GaN Thickness and Uniformity

As shown in the simulation of Figure 3c,d, the angular dependence of the far-field emission is strongly influenced by the p-GaN thickness due to the presence of the backside mirror but also, to a lesser extent, by the n-GaN thickness. The p-GaN thickness is defined during growth and should be quite uniform across the wafer. However, when designing the epi-structure, it is challenging to precisely tune the half-cavity (p-GaN + nid-GaN in our model) due to uncertainties in parameters such as the refractive indices of the materials and the phase shift at the p-GaN-mirror interface. Therefore, having a precise characterization method to match the simulation and adjust the input parameters is very useful. Additionally, we know that during the GaN buffer thinning by dry etching, some total thickness variation (TTV) is introduced across the wafer due to non-uniformities inherent to the etching tool. We attribute the variation in directivity between different dies, as presented in Figure 5a, to the variation in n-GaN thickness. To confirm this hypothesis, we measured the far-field angular distributions for six spectral slices (from 430 to 480 nm) and compared them to the best-fit simulations. As shown in Figure 4d, Figure 5b, and Figure 5c for Dies 1, 2, and 3, respectively, the simulations reproduce the experimental curves quite well. The optimum fitting parameters (gathered at the table in Figure 5e) confirm that the thickness of p-GaN + nid-GaN varies by less than 5 nm (between 202 and 207 nm), whereas the thickness of n-GaN + nid-GaN varies more significantly, by 65 nm, from 634 to 699 nm. These values are consistent with the fact that, in our process, the GaN thickness after substrate removal and cavity thinning is usually thinner at the center. Furthermore, reflectivity measurements were conducted precisely at the center of the wafer following the substrate removal and the GaN thinning process. These measurements revealed a total GaN thickness of 836 nm in perfect agreement with the wavelength-dependent emission diagram fit presented in Figure 4. In future studies, to confirm that this approach predicts GaN thickness so accurately, a comparison between the measured GaN thickness and the value extracted from the angular dependence of far-field emission should be repeated at multiple locations across the wafer.

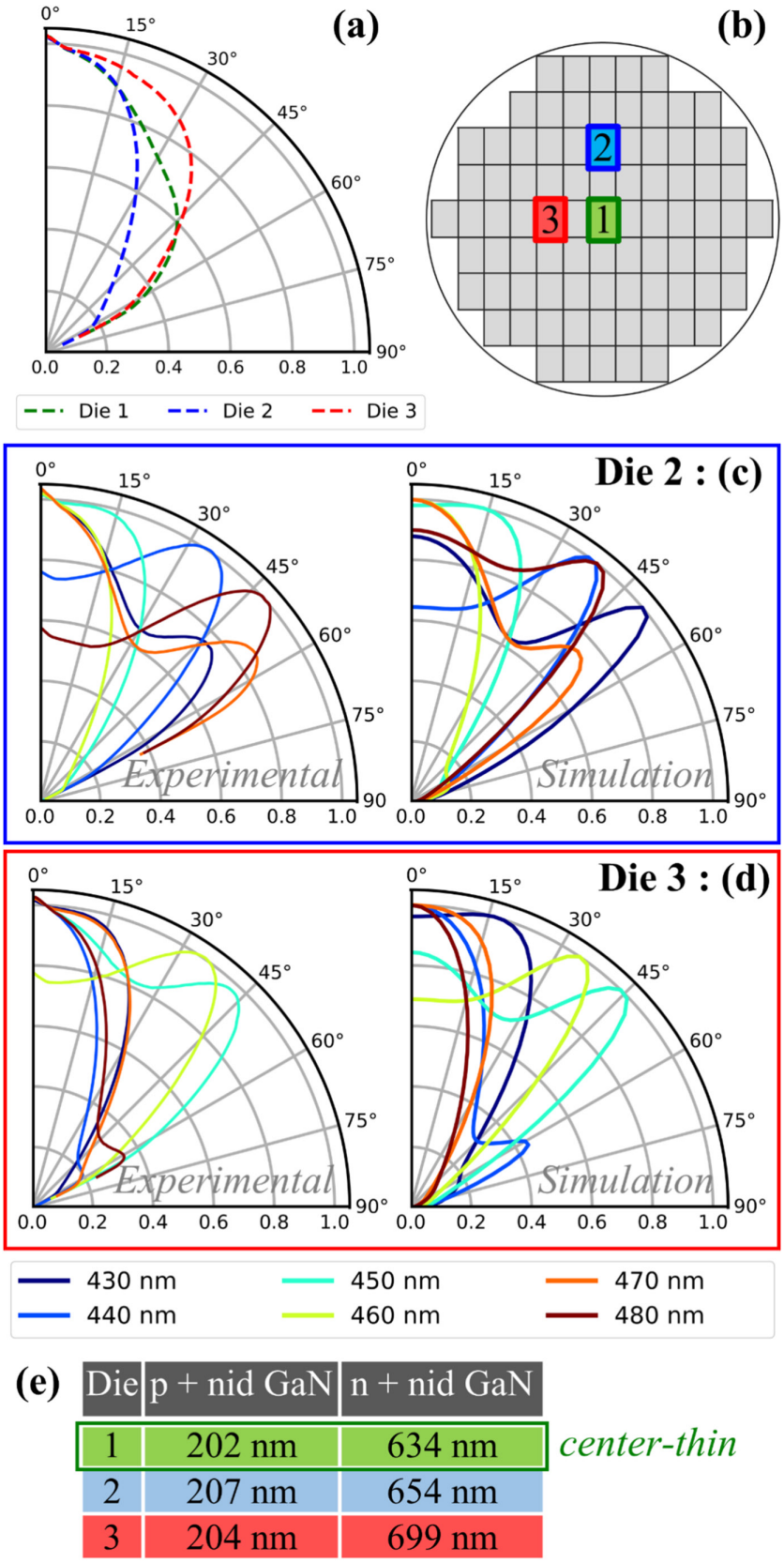

(e)

Die	p + nid GaN	n + nid GaN	
1	202 nm	634 nm	*center-thin*
2	207 nm	654 nm	
3	204 nm	699 nm	

FIGURE 5 | (a) Angular dependence of far-field EL emission of 200-μm disk LED, driven at approximately 30A/cm^2, and measured for three dies located at different positions on the 200-mm wafer, as described in (b). Angular dependence of the far-field emission contributions from the various wavelengths composing the spectrum for (c) Die 2 and (d) Die 3. As for the Die 1 in Figure 4d, the simulation describes the experimental data quite well by primarily adjusting the thickness of n-GaN + nid-GaN, which varies due to the etch thinning step. (e) Table summarizing the thicknesses obtained from the best-fit simulations.

This study emphasizes the importance of precisely controlling the overall optical cavity thickness to achieve uniform and directional emission across the entire wafer, as a TTV of less than 100 nm is already quite good and the result of a well-controlled process.

3.2 | Light Extraction Efficiency (LEE)

In addition to directivity, cavity effects significantly influence the LEE. Figure 6a illustrates the total LEE as a function of n-GaN + nid-GaN and p-GaN + nid-GaN thicknesses, with the nid-GaN thickness fixed at 25 nm, as modeled in Figure 3a. The p-GaN thickness has a more pronounced impact on LEE compared to the n-GaN thickness, similar to its effect on directivity. To maximize LEE, the p-GaN thickness should be around 230 nm, indicating that our current sample is not optimal. By increasing the p-GaN thickness by 25 nm, we could expect to nearly double the LEE.

This imperfect tuning of the cavity may stem from inaccuracies in the refractive indices used in the modeling or from minor integration changes not accounted for in the initial simulation. It is also important to note that LEE varies with the emission wavelength, as shown in Figure 6b. Therefore, the cavity configuration will only be optimal for a specific range of wavelengths. Additionally, we want to emphasize that in these simulations of LEE using the Setfos software, the Purcell effect is well accounted for, to compute the total emitted power. In these simulations, we assumed an IQE equal to unity, thus eliminating its impact on the efficiency of the LED. The zoomed-in view of Figure 6a highlights the variation in LEE as the n-GaN thickness changes, with an adjusted color scale for better visibility. Although less pronounced than the impact of p-GaN, the oscillating variation of LEE is still significant. This analysis underscores the importance of the epi-structure design on both LEE and directivity. By coupling far-field characterizations as a function of wavelength and angle with an accurate 1D modeling, we can refine the optimal thicknesses for the different layers to enhance performance. Even if the initial simulation were to be inaccurate due to a lack of precise refractive index parameters, the thicknesses could be adjusted in a second iteration of micro-LED fabrication. It would then be desirable to always include some larger LEDs on wafers used for micro-LED-based devices, such as micro-displays, to monitor cavity tuning, similar to how we typically add TLM structures for contact monitoring. As we will see in the final section, even though a 1D model does not account for the effects of sidewalls on far-field emission, it describes the directivity of micro-LEDs of 5 μm and larger rather well. For some applications, such as micro-LED-based data communication, a size of 10 μm is perfectly reasonable for ongoing development and is adequately described by a 1D model. It is also important to remind that for practical applications, it is crucial to maximize the LEE within a specific emission cone angle determined by the application, rather than just the total LEE.

3.3 | Forward Bias

Figure 7a demonstrates that the angular dependence of far-field EL emission changes as the forward bias driving a

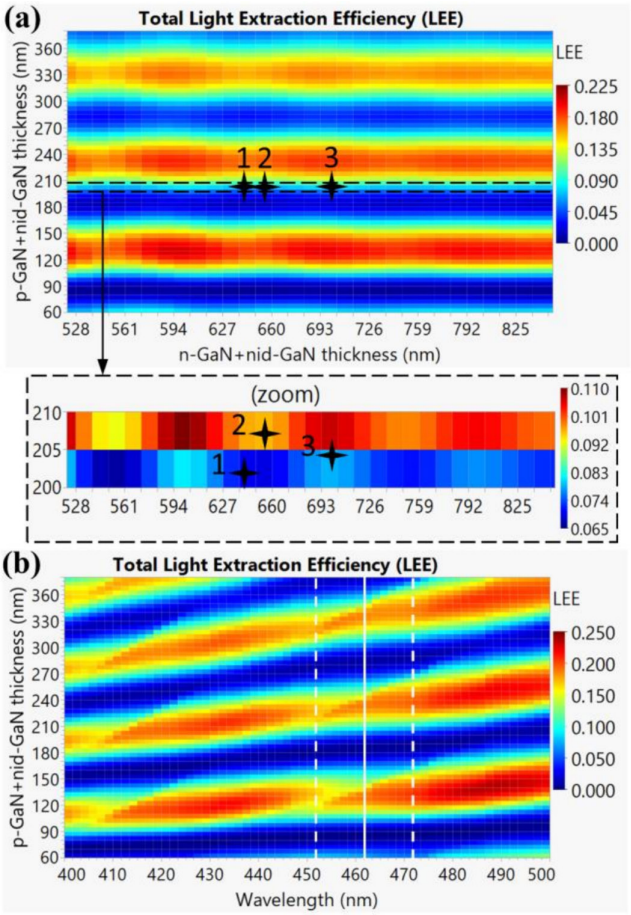

FIGURE 6 | (a) Simulation results of the total light extraction efficiency (LEE) as a function of p-GaN + nid-GaN and n-GaN + nid-GaN thicknesses, based on the model in Figure 3a. The nid-GaN thickness remains constant at 25 nm for all simulations. The spectrum used for these simulations is a typical one for our LEDs centered around 460 nm. Dies 1, 2, and 3, whose emission diagrams were presented in Figure 4d and Figure 5c,d, are marked as crosses in the mapping. The zoomed-in view, framed with dotted lines, focuses around the p-GaN thickness of the three dies. By adjusting the color scale, the oscillating variation of LEE with n-GaN thickness becomes clear, although it is less pronounced than for p-GaN. (b) Total LEE as a function of p-GaN + nid-GaN and wavelength. The white line indicates the peak position of the spectrum in Figure 4a, and the dotted lines represent the wavelengths at half maximum.

200-μm disk LED increases. This may initially seem surprising, as light extraction is mainly related to material properties. However, it is well known that the InGaN/GaN QW spectra exhibit a blue shift with increasing injected current. This phenomenon is due to the presence of a strong internal electric field in the QW, resulting from a polarization mismatch at the InGaN/GaN interfaces. This internal field red-shifts the luminescence through the quantum-confined stark effect (QCSE). The injection of carriers into the QWs can partially self-screen this internal field, leading to a blue shift, as illustrated in Figure 5d. Due to the strong wavelength dependence of directivity, this blue shift likely causes the modification in the angular dependence of the far-field EL emission shown in Figure 7a. Although contributions from other QWs (besides the first one on the p-GaN side) could also affect directivity

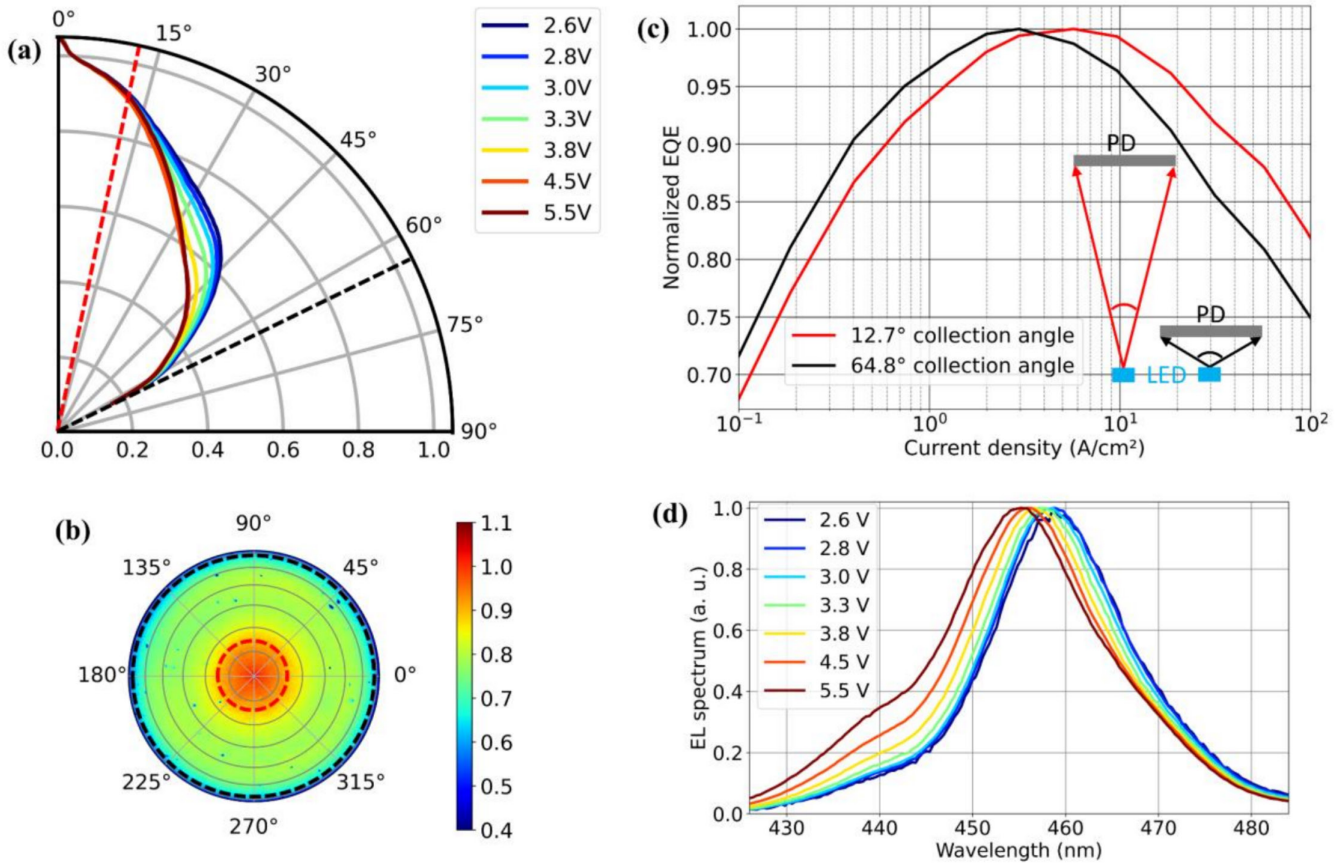

FIGURE 7 | (a) Angular dependence of the far-field EL emission of a 200-μm disk LED as the applied forward bias varies. (b) 2D emission diagram in (θ, φ) with red and black dotted circles defining the integration limits for external quantum efficiency (EQE) calculation. This example corresponds to V = 3.3 V. (c) Normalized EQE versus current density of the device, plotted for two limit collection angles: 12.7° (red) and 64.8° (black), as described in the inset. Reducing the collection angle gives the impression that the EQE peaks at a higher current density. (d) Normalized EL spectra corresponding to the emission diagram in (a), showing the typical blue shift attributed to the screening of the internal electric field.

as the applied bias changes, this impact is expected to be limited [14].

An important implication of this voltage or current dependence of the emission diagram is that it induces variations in the light collected within a specific solid angle of a system. For microdisplay applications, where pixels are dimmed by pulse-width modulation (PWM), the impact should be minimal as the driving current density is kept constant. However, for applications that require varying injected currents, the proportion of photons collected within a given solid angle, relative to the total number of photons emitted, will not remain constant. This is particularly important for the on-wafer characterization of EQE, which is a key figure of merit in micro-LED development. Because measuring micro-LEDs in an integrating sphere is challenging (due to the need for dicing, packaging, and the low power output relative to noise levels), the optical power of a micro-LED is typically measured with a photodiode at a sufficient distance to allow for on-wafer probing. This setup imposes a limit on the collection angle, as illustrated in the inset of Figure 7c. In this figure, we plot the normalized EQE versus current density for the same 200-μm disk LED as in Figure 7a. We compare the EQE extracted from the center of the emission diagram (up to 12.7°) with the EQE extracted from all the light collected by our objective with NA = 0.9, imposing a limit angle of 64.8°, as described in Figure 7b. In this specific device, reducing the solid angle makes it appear as though the EQE peaks at a higher current density J_{max}. This can be misleading, as this value of J_{max} is often used to indicate a change in non-radiative recombination levels. Indeed, in a simplistic ABC model, often used to describe the current density dependence of EQE, if the radiative and Auger recombination parameters (B and C, respectively) remain constant and only the Shockley–Read–Hall (SRH) parameter A changes, an increase in A shifts the normalized EQE peak to a higher current density [18]. This current density dependence of the LEE can then complicate the analysis of micro-LED performance. Again, this effect was illustrated using a macro-LED (200 μm), as it can be more easily modeled by 1D simulations. However, as we will see in the next section, the impact of cavity effects remains significant even for micro-LEDs with dimensions of just a few micrometers. Therefore, this change in LEE with current density would also impact the study of small micro-LEDs.

3.4 | Micro-LED Size

All the results presented previously were obtained using 200-μm disk LEDs because we fitted the results with a 1D simulation model. We can consider a 200-μm disk to be equivalent to an infinite LED, as the impact of sidewalls on directivity is minimized due to the large perimeter-to-surface ratio.

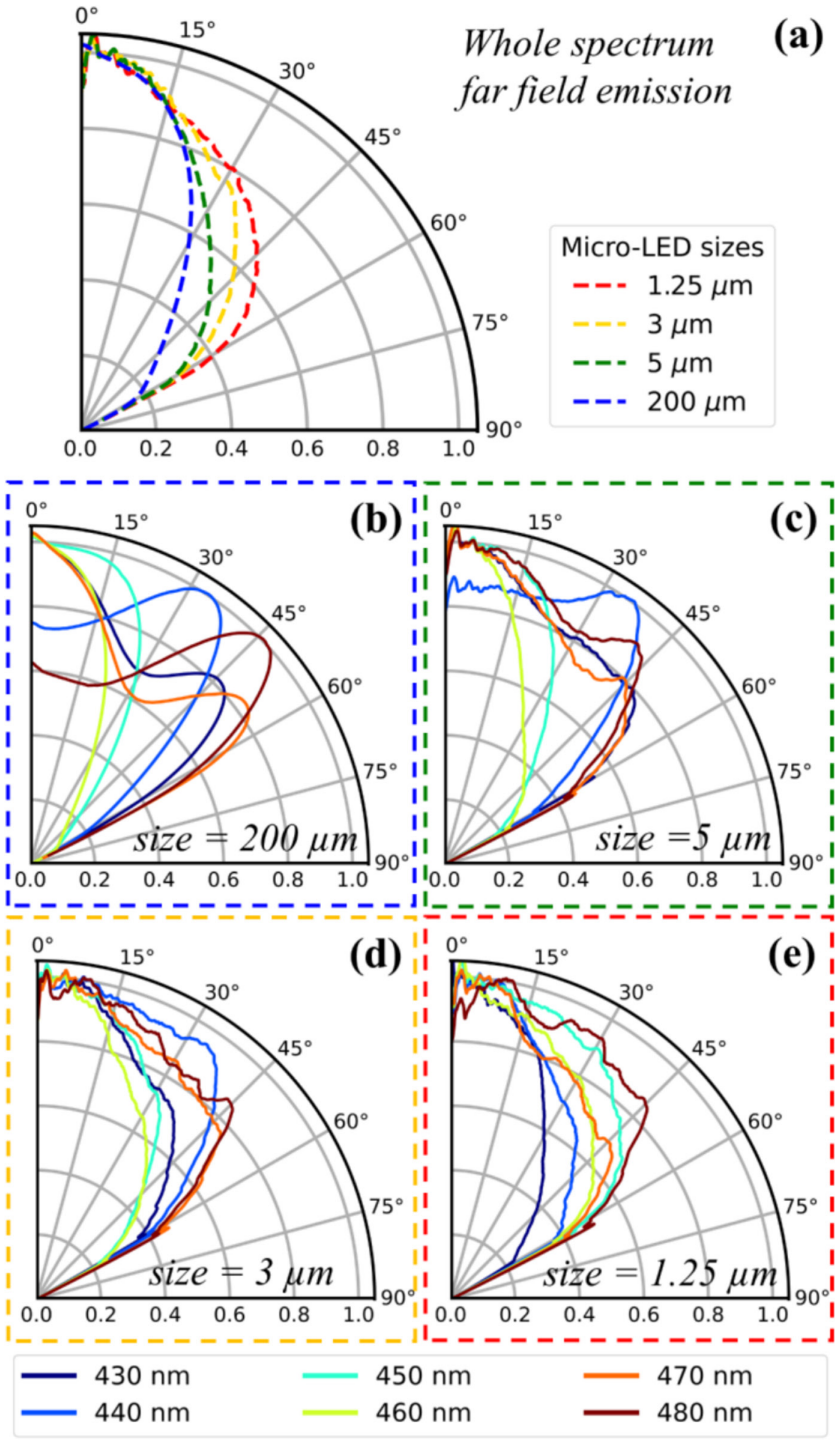

FIGURE 8 | Angular dependence of far-field EL emission measured for four micro-LEDs of sizes: 200, 5, 3, and 1.25 μm. All LEDs are located on Die 1 and in close proximity, driven with a similar current density of 30 A/cm^2 for each size. The 1.25-μm micro-LED has a central n-contact, whereas the three larger ones have a peripheral contact. Consequently, the far field of the smallest micro-LED may not be comparable to the others, both due to this difference in contact geometry and its smaller size. (a) Measurement with the whole spectrum. (b–e) Spectral decomposition of the emission diagram.

This approach made it easier to visualize cavity effects and their impact on various aspects of micro-LED studies. Now, it is important to study the impact of micro-LED size on the angular dependence of far-field emission. To achieve this, we compared the emission diagram of the 200-μm disk LED (the reference macro-LED) with disk micro-LEDs of 5, 3, and 1.25 μm in diameter.

Figure 8a illustrates how the directivity of EL emission changes as the size of the micro-LED decreases. For these measurements, all LEDs are from the same die and closely located, minimizing the average TTV among the devices. We selected a 200-μm LED that exhibits directional emission. However, as the size of the micro-LEDs decreases, they progressively lose this directivity, probably due to the impact of the sidewalls. However, there are

two important points to mention: First, the smallest micro-LED of 1.25 μm has a central n-contact, whereas the three larger ones have a peripheral contact. Therefore, we can likely compare the far-field emission of the 200-, 5-, and 3-μm micro-LEDs. However, it is less clear whether the 1.25-μm micro-LED can be compared directly. Thus, the difference in far-field emission for this very small micro-LED could be due to the impact of the sidewalls or a change in n-contact geometry. Secondly, the emission diagram of Figure 8a are measured for the same current density. However, the spectra (not shown in this paper) exhibit a small red shift from 455 to 460 nm as the size of the micro-LED decreases from 200 to 1.25 μm. This effect could be due to possible leakage paths (or defect-related parallel diode) at the sidewalls or strain relaxation impacting the internal electric field. Such an effect would create differences in the emission diagrams of the various micro-LED sizes when considering the entire spectrum, even for an identical spectral decomposition, potentially amplifying the differences as observed in Figure 8a. Figure 8b–e displays the wavelength decomposition of the angular distribution of far-field EL emission for the four micro-LEDs of different sizes. This decomposition offers more detailed insights than the whole spectrum, and we are less affected by the spectrum wavelength shifts. The emission diagrams for each wavelength in the 5-μm LED retain similar shapes to those of the 200-μm LED, though less pronounced. Even though the far-field emission of the 3-μm micro-LED significantly deviates from that of the large LED (and the associated 1D model), we observe that the most directional emission wavelength remains at 460 nm. There appears to be a residual impact of the 1D cavity effect, increasingly influenced by the sidewalls. This suggests that the sidewalls of small micro-LEDs play a role as crucial as the vertical optical cavity. The measurement of the 1.25-μm micro-LEDs demonstrates our ability to measure the far-field angular distribution for very small emitters. However, as previously discussed, it cannot be directly compared to the others. In this case, the emission at 430 nm is the most directional. This suggests that achieving directional emission from small micro-LEDs is still possible, but the cavity thicknesses must be adjusted to match the dominant emission wavelength of the micro-LED. Therefore, optimizing in 3D the design of micro-LEDs smaller than 5 μm will likely require 3D-FDTD simulations to account for both sidewall effects and vertical cavity effects [19, 20].

4 | Conclusion

We have developed a setup to measure the angular dependence of the far-field EL emission of micro-LEDs, considering either the whole spectrum or specific wavelengths. The experimental data obtained from flip-chip micro-LEDs fabricated on 200-mm wafers were compared to 1D Setfos simulations, allowing us to determine the various thicknesses composing the device structure. The wavelength decomposition of the emission diagram enables an accurate fit between experimental data and simulations, as the far-field pattern varies significantly with wavelength. This study revealed that the p-GaN thickness was not optimal for maximizing the total LEE. Additionally, the LED TTV, resulting from the n-GaN thinning process, affects the emission directivity of 200-μm disk LEDs, making these devices very suitable for process monitoring and optimization. Actually, it would be beneficial to always include large LEDs on micro-LED-based wafers to monitor cavity tuning and dispersion both within and between wafers, particularly, as we were able to verify that the 1D cavity effects continue to control the emission diagram even for LEDs as small as 5 μm. Experimentally, we observed that the angular dependence of the far-field emission changes with the applied forward bias, likely due to the wavelength shift caused by the screening of the internal field. This has direct implications for on-wafer EQE characterization, commonly used in micro-LED development. Specifically, the LEE within a given collection angle varies with the applied bias, potentially altering the EQE versus current density curve. Finally, we characterized micro-LEDs of various sizes and observed that the emission diagram progressively deviates from that of larger LEDs, which are primarily controlled by the optical cavity. However, even at 5 μm, the angular distribution of far-field emission remains quite similar to that of larger LEDs. We were also able to perform measurements on very small micro-LEDs of 1.25 μm, which exhibited a different emission diagram with an optimum directivity occurring at a different wavelength. These results still demonstrate the possibility of achieving directional emission with small micro-LEDs. The differences in far-field emission could be due to the different n-contact geometry, as well as the sidewalls, which are expected to play a major role at these small dimensions. To design more directive micro-LEDs smaller than 5 μm, 3D-FDTD simulations will be necessary to account for both vertical cavity effects and sidewall influences.

Acknowledgments

This work is part of the IPCEI Microelectronics and Connectivity and was supported by the French Public Authorities within the frame of France 2030.

Data Availability Statement

The data that support the findings of this study are available from the corresponding author upon reasonable request.

References

1. V. Kumar and I. Kymissis, "MicroLED/LED Electro-Optical Integration Techniques for Non-Display Applications," *Applied Physics Reviews* 10, no. 2 (2023): 021306.

2. A. Cibié, S. El Badaoui, P. Le Maitre, et al., "Parallel Communication With InGaN/GaN Micro-LEDs Using a CMOS Compatible Approach," in *Light-Emitting Devices, Materials, and Applications XXVIII [Internet]*, eds. J. K. Kim, M. R. Krames, and M. Strassburg (SPIE, 2024), https://doi.org/10.1117/12.3002681.

3. P. Le Maitre, A. Cibié, F. Rol, et al., "Short Range Optical Communication With GaN-On-Si microLED and microPD Matrices," *Journal of the Society for Information Display* 32, no. 12 (2024): 797–814.

4. Z. Li, L. Yu, B. Liu, et al., "High-Speed Micro-LEDs Based on Nano-Engineered InGaN Active Region Towards Chip-to-Chip Interconnections," *Journal of Lightwave Technology* 42, no. 24 (2024): 8760–8770.

5. B. Pezeshki, F. Khoeini, A. Tselikov, R. Kalman, C. Danesh, and A. Afifi, "MicroLED Array-Based Optical Links Using Imaging Fiber for Chip-to-Chip Communications," in *Optical Fiber Communication Conference (OFC) 2022 [Internet]*, (Optica Publishing Group, 2022) [cited 2025 Mar 26], p. W1E.1, https://opg.optica.org/abstract.cfm?URI=OFC-2022-W1E.1.

6. P. R. West and K. Ahmed, "21-5: Far-Field Native Emission Patterns of Various MicroLED Structures," *SID Symposium Digest of Technical Papers* 54, no. 1 (2023): 283–286.

7. F. Templier, "GaN-Based Emissive Microdisplays: A Very Promising Technology for Compact, Ultra-High Brightness Display Systems: GaN-Based Emissive Microdisplays," *Journal of the Society for Information Display* 24, no. 11 (2016): 669–675.

8. F. Templier, L. Benaïssa, B. Aventurier, et al., "19-6: Invited Paper: A Novel Process for Fabricating High-Resolution and Very Small Pixel-Pitch GaN LED Microdisplays," *SID Symposium Digest of Technical Papers* 48, no. 1 (2017): 268–271.

9. D. Dominguez, N. Alharbi, M. Alhusain, A. A. Bernussi, and L. G. de Peralta, "Fourier Plane Imaging Microscopy," *Journal of Applied Physics* 116, no. 10 (2014): 103102.

10. T. Fujii, A. David, C. Schwach, et al., "Micro Cavity Effect in GaN-Based Light-Emitting Diodes Formed by Laser Lift-Off and Etch-Back Technique," *Japanese Journal of Applied Physics* 43, no. 3B (2004): L411–L413.

11. H. Benisty, H. De Neve, and C. Weisbuch, "Impact of Planar Microcavity Effects on Light Extraction-Part I: Basic Concepts and Analytical Trends," *IEEE Journal of Quantum Electronics* 34, no. 9 (1998): 1612–1631.

12. Y. C. Shen, J. J. Wierer, M. R. Krames, et al., "Optical Cavity Effects in InGaN/GaN Quantum-Well-Heterostructure Flip-Chip Light-Emitting Diodes," *Applied Physics Letters* 82, no. 14 (2003): 2221–2223.

13. R. Chance, A. Prock, and R. Silbey, "Molecular Fluorescence and Energy Transfer Near Interfaces," *Advances in Chemical Physics* 37 (1978): 1–65.

14. A. David, M. J. Grundmann, J. F. Kaeding, N. F. Gardner, T. G. Mihopoulos, and M. R. Krames, "Carrier Distribution in (0001)InGaN/GaN Multiple Quantum Well Light-Emitting Diodes," *Applied Physics Letters* 92, no. 5 (2008): 053502.

15. S. L. Chuang and C. S. Chang, "k·p Method for Strained Wurtzite Semiconductors," *Physical Review B* 54, no. 4 (1996): 2491–2504.

16. L. Schade, U. T. Schwarz, T. Wernicke, M. Weyers, and M. Kneissl, "Impact of Band Structure and Transition Matrix Elements on Polarization Properties of the Photoluminescence of Semipolar and Nonpolar InGaN Quantum Wells," *Physica Status Solidi B: Basic Solid State Physics* 248, no. 3 (2011): 638–646.

17. M. Regnat, K. P. Pernstich, S. Züfle, and B. Ruhstaller, "Analysis of the Bias-Dependent Split Emission Zone in Phosphorescent OLEDs," *ACS Applied Materials & Interfaces* 10, no. 37 (2018): 31552–31559.

18. A. David, N. G. Young, C. Lund, and M. D. Craven, "Review—The Physics of Recombinations in III-Nitride Emitters," *ECS Journal of Solid State Science and Technology* 9, no. 1 (2020): 016021.

19. F. Vögl, A. Avramescu, F. Knorr, et al., "Role of Pixel Design and Emission Wavelength on the Light Extraction of Nitride-Based Micro-LEDs," *Optics Express* 31, no. 14 (2023): 22997–23007.

20. F. Vögl, A. Avramescu, S. Gelfert, et al., "Optical Characteristics of Thin Film-Based InGaN Micro-LED Arrays: A Study on Size Effect and Far Field Behavior," *Optics Express* 32, no. 10 (2024): 17644–17656.

Biographies

Fabian Rol is a senior scientist at the CEA-LETI Institute in Grenoble, France. He graduated from ESPCI (Ecole Supérieure de Physique et de Chimie Industrielles de la Ville de Paris) and received a master's degree in solid-state physics and condensed matter from the University of Paris-Saclay in 2003. He obtained a PhD in Physics from the University of Grenoble-Alpes in 2007. Since then, he has worked extensively in the field of nitride semiconductor emissive devices and photonic structures, first at UCSB (University of California, Santa Barbara) and Harvard University in the group of Professor Hu until 2010 and later in the industry at CREE Inc. (now Wolfspeed Inc.). He joined CEA-LETI in 2019 to work on the development of GaN-based micro-LEDs.

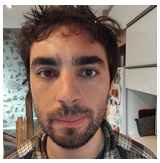

Stéphane Altazin is a research scientist at CEA-LETI, specializing in optoelectronics with a particular focus on micro-LEDs. His research interests lie in the development and optimization of micro-LED technologies for various applications. Dr. Altazin completed his thesis on the modeling of charge transport in organic semiconductor devices, contributing significantly to the field of organic electronics. Prior to joining CEA-LETI, Dr. Altazin served as a product manager for software solutions at Fluxim, where he gained valuable experience in managing and developing advanced simulation tools for optoelectronic devices. Additionally, he has worked as a device engineer for bolometers at Lynred, a leading company in infrared imaging technology. His role involved developing and optimizing bolometer detectors used in thermal cameras, enhancing their sensitivity and performance.

Nicolas Michit received his engineering degree from Centrale Nantes in 2016 and his PhD in silicon photonics at the Institute of Nanotechnologies of Lyon in 2020. Since 2020, he has been working with CEA LETI Institute as a research engineer, focusing on the optical modeling of GaN-based emissive devices.

Bastien Miralles was born in Montpellier, France. He received his engineering degree from Polytech Grenoble in 2018. He joined the CEA-LETI Institute in 2019, working on the integration of GaN micro-LEDs.

Clément Ballot received his engineering degree in material sciences from Grenoble-INP Phelma, located in Grenoble, France, in late 2017. Since 2018, he has been working at the CEA-LETI Institute in France as a research engineer, focusing on the process integration of GaN-based emissive devices for microdisplay applications and optical communications.

Bernard Aventurier was born in Grenoble, France. He received a master's degree from Joseph Fourier University in Grenoble in 1993. He studied and developed new infrared detector technology at the CEA-LETI in Grenoble until 2003 in collaboration with SOFRADIR (now INRED). For the next 4 years, he worked on the technology of thin-film transistors using low-temperature processes on glass and flexible substrates. During the years 2008–2017, he focused his activity on the development of OLED display in collaboration with Microoled. Since 2017, he is currently focused on developing process integration for GaN-based micro-LED and OLED technologies.

Paolo De Martino joined CEALETI, Grenoble, France, just after receiving his master's degree in nanotechnologies for ICTs, Politecnico di Torino, in 2020. His research interest spreads from the integration up to the device understanding of LEDs for display applications. He worked both on phosphorus and III-N-based light-emitting semiconductors for microdisplay and optical communication applications. From 2022, he is also responsible for leading several explorative research projects.

Patrick Le Maitre was born in Caen, France. He received his engineering degree from Supélec (now CentraleSupélec, France) in 2000 and a master of engineering degree from the Tokyo Institute of Technology in 2001. He joined Renesas Technology in 2001 and then moved to NXP Semiconductor in 2004. In 2010, he joined STMicroelectronics in Crolles, focusing on the development of Silicon photonics platforms. Since 2019, he has been a research engineer at the CEA-LETI Institute in France, developing GaN-based emissive devices for microdisplay applications and optical communications.

Julia Simon, senior scientist in CEA-LETI, graduated in physics from the Polytechnique Institute of Grenoble (INPG) in 1998. She obtained her PhD in solid-state physics in 2001 dealing with optical properties of GaN-based heterostructures grown by MBE. Research engineer in advanced photolithography in CEA-LETI from 2001 to 2009, she has gained strong expertise in the area of integration technologies and processes. In 2009, she joined CEA/LITEN, where she took charge of the R&D development of thermoelectrics (20 persons) in a large industrial project until 2014. She moved back to the optical department of LETI, where she is now in charge of the technological integration and device performance of high-resolution micro-LED arrays for industrial partners in micro-display and optical communication applications.